**ADVANCED
SCIENCE NEWS**
www.advancedsciencenews.com

**ADVANCED
MATERIALS
TECHNOLOGIES**
www.advmattechnol.de

FULL PAPER

Lenticular-Lens-Based Colored Antiglare Dashboard Surfaces

*Chengang Ji, Guodong Zhu, Cheng Zhang, Sunghyun Nam, Qiaochu Li, Liangping Xia,
Weiguo Zhang, Debasish Banerjee,* and Lingjie Jay Guo**

All current vehicle dashboards are black in order to prevent any veiling glare
that interferes safe driving. Here, the authors report on a novel design of sur-
face that can impart color to the dashboard and does not cause veiling glare
to the driver. This is made possible by covering a substrate with alternating
absorber/colored stripes with specially designed lenticular lens arrays, where
reflected light rays are controlled out of the veiling glare range while at the
same time create visual colors to drivers. As an experimental demonstration,
a 3.5 cm² square sample is fabricated by imprinting method. The presented
approach provides a new application of lenticular lenses and can be poten-
tially applied to embellish vehicles' interiors. Due to the small pitches
(≈50 µm) of lenses, the proposed method can even be extended for vehicle
displays with high resolutions if integrating with active devices.

1. Introduction

In recent years, vehicles with colored interior decorations, which
are appealing to consumers, have taken a considerable market
share.[1,2] Various materials, such as fabric, leather, and vinyl, are
commonly used for the colored interiors.[1] Although the vehicle
interior decorations improve steadily in the past, the dash-
board under the windshield is always black to avoid the issue
of veiling glare. The veiling glare is a ghost image of the vehicle
dashboard created by reflection from the windshield and pro-
jected into the drivers' eyes (**Figure 1**a). This projected image
disturbs the driver's visual field and thus creates potential safety
issues due to the reduced visibility of objects ahead.[3–8]

There have been past efforts to design
dashboard surfaces that can produce
desired colors, and at the same time, avoid
veiling glare. For example, a veiling reduc-
tion system which integrates absorption-
type polarizers and reflective color filters
beneath has been proposed.[9,10] However,
the brightness of the dashboard is limited
by the absorption nature of the polarizer.
This issue can be mitigated by replacing
the absorption-type polarizers with reflec-
tion type wire grid polarizers,[11] which
increases the reflection brightness from
dashboards and eases the requirement for
the lamination of reflective color filters
and polarizers.

In this work, we report a design based
on lenticular lens arrays that can enable colored dashboard,
which shows desirable colors and at the same time, avoids
veiling glare. This is achieved by laminating an alternating
absorber/colored stripe substrate underneath a lenticular lens
array with specific dimensions, where the light in the veiling
glare range is absorbed by the black stripes leaving light from
colored stripes reaching driver's eye. As an experimental dem-
onstration, a 3.5 cm × 3.5 cm size sample with the lens pitch of
50 µm is fabricated by using thermal imprinting,[12–14] which
represents a low cost manufacturing method. Due to the small
period of the fabricated lenses, the lens array can be potentially
extended to a display system with high resolution if replacing
the stripes with active light emitting devices.

C. Ji, Dr. C. Zhang, Q. Li, Prof. L. J. Guo
Department of Electrical Engineering
and Computer Science
The University of Michigan
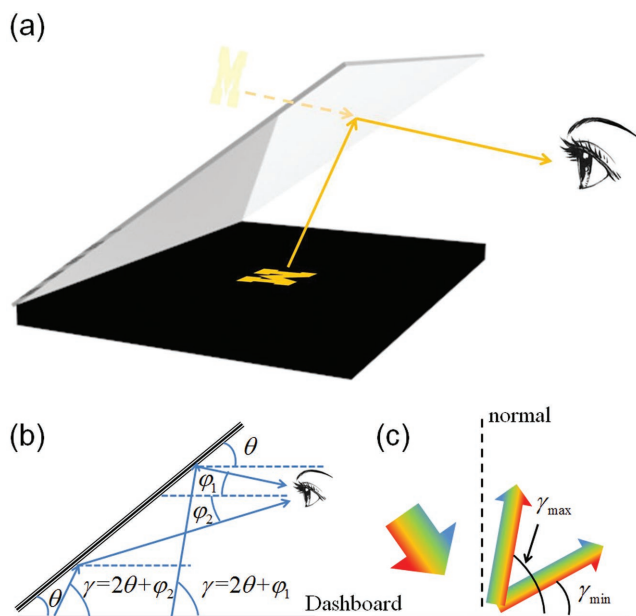Ann Arbor, MI 48109, USA
E-mail: guo@umich.edu
Dr. G. Zhu, Dr. L. Xia, Dr. W. Zhang
Key Laboratory of Multi-Scale Manufacturing Technology
Chongqing Institute of Green and Intelligent Technology
Chinese Academy of Sciences
Chongqing 400714, China
S. Nam, Prof. L. J. Guo
Macromolecular Science and Engineering
The University of Michigan
Ann Arbor, MI 48109, USA
Dr. D. Banerjee
Toyota Motor Engineering and Manufacturing North America
Ann Arbor, MI 48105-9748, USA
E-mail: debasish.banerjee@toyota.com

2. Antiglare with Lenticular Lenses

2.1. Veiling Glare Angular Range of Windshield-Dashboard System

A simplified windshield-dashboard system is depicted in
Figure 1b. The rake angle θ of the dashboard system, which
is defined as the angle between the windshield and the dash-
board, ranges from 25° to 35° for different vehicle models. The
rake angle plays an important role affecting the veiling glare as
the reflectivity increases with the incident angles of light onto
the windshield glass according to the Fresnel equations as
plotted in Figure S1 (Supporting Information). Light reflected
from the windshield into drivers' eyes causes the veiling glare.
In practice, the driver usually has a viewing angle φ of ±15°
with respect to the horizontal direction (Figure 1b). It is the
reflected light falling into drivers' viewing angle that produces
the veiling glare. Here, the positive value φ (designated as

**ADVANCED
MATERIALS
TECHNOLOGIES**
www.advmattechnol.de

**ADVANCED
SCIENCE NEWS**
www.advancedsciencenews.com

Figure 1. Veiling glare angular range calculation with the rake angle θ and the direction of light rays from windshield φ. a) The definition of the veiling glare effects. b) A schematic diagram draws a relation between reflection angle from dashboard γ and θ, φ as $\gamma = 2\theta + \varphi$. c) Veiling glare range for vehicles with different rake angles varies between $\gamma_{min} = 2\theta - 15°$ and $\gamma_{max} = 2\theta + 15°$ with θ ranging from 25° to 35°. The whole veiling glare range lies in the right half plane with respect to the normal of the incident plane.

φ_1 in the plot) corresponds to the light coming from above the horizontal direction, while the negative φ (i.e., φ_2) from below. Veiling glare becomes a serious issue if the dashboard is not covered with black absorbing material, as one experience when placing a piece of white paper on the dashboard, which causes strong reflected light into the driver's eyes.

The veiling glare angle γ is the angle where the reflected light from dashboard will enter the view field of drivers, leading to a veiling glare. It is related to the rake angle θ and the viewing angle φ as $\gamma = 2\theta + \varphi$. Considering drivers' viewing angle φ of ±15°, the veiling glare angular range is calculated to be $\gamma_{min} = 2\theta - 15°$ to $\gamma_{max} = 2\theta + 15°$. Considering the value of θ (from 25° to 35°), γ lies in the right half plane as shown in Figure 1c. For an antiglare dashboard, the reflection needs to be suppressed in the angular range between γ_{min} and γ_{max}.

2.2. Lenticular Lens Arrays

Lenticular lenses are cylindrical periodic lens arrays that provide different magnified images at different angles. They are commonly integrated in 3D printing and electronic displays to create special visual effects (e.g., animation and depth of illusion) by controlling light propagation with curved shapes.[15–20] By using lenticular lenses, different images are observed with

different viewing positions. As illustrated in **Figure 2**a, if lenticular lens array is placed on top of alternating colored stripes, the bright colored (yellow) stripe can be viewed on the left side with respect to the normal, while the dark color can be observed from the right half.
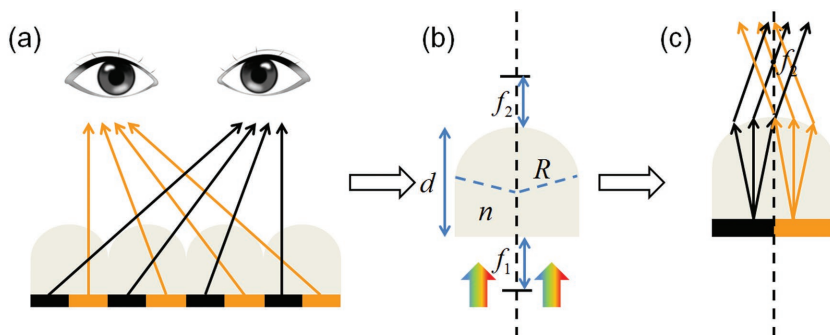
The property of the lenticular lenses can be simply explained using the ABCD transfer matrix method. The transfer function $\overline{M}$ of a single lenticular lens is[21]

$$\overline{M} = \begin{pmatrix} 1 & 0 \\ -\dfrac{1-n}{R} & n \end{pmatrix} \begin{pmatrix} 1 & d \\ 0 & 1 \end{pmatrix} \begin{pmatrix} 1 & 0 \\ 0 & \dfrac{1}{n} \end{pmatrix}$$

$$= \begin{pmatrix} 1 & \dfrac{d}{n} \\ -\dfrac{1-n}{R} & 1-d\dfrac{1-n}{nR} \end{pmatrix} \tag{1}$$

where d is the thickness of the lens, n is the refractive index of the lens constituent material, and R is the radius of the curved dome. R is a negative value when light coming from the bottom side (Figure 2b). The three matrices in the calculation of $\overline{M}$, from right to left, correspond to the light refraction at the interface between the air and the flat bottom plane of the lens, light propagation within the lens, and the refraction between the top dome and the air, respectively. It should be noted that Equation (1) is valid in cases where the curvature of top surface is relative small compared to the thickness of the lens. More accurate analysis can be performed with ray-tracing method, which is discussed in Section 3. Based on Equation (1), the bottom and top focal lengths f_1 and f_2 can be obtained as

$$f_1 = \frac{R}{1-n} - \frac{d}{n}, \quad f_2 = \frac{R}{1-n} \tag{2}$$

For a typical lenticular lens, the bottom focal plane overlaps with the flat bottom plane of the lens, i.e., $f_1 = 0$. Based on this condition, the thickness d is related to the radius R and the refractive index n as

Figure 2. Physical explanation of the light guidance property of the lenticular lenses. a) Different images can be observed when viewed from different angles and this contributes to the various visual effects created with the lenticular lens array. b) Analysis of the dimension of a single lenticular lens. The thickness of the lens d can be expressed with the refractive index n and the radius R as $d = nR/(1 - n)$. c) Schematic of refraction of light rays coming from the bottom side. The light from the colored area will be directed to the left half and the light from the dark area is refracted to the right.

ADVANCED
SCIENCE NEWS
www.advancedsciencenews.com

ADVANCED
MATERIALS
TECHNOLOGIES
www.advmattechnol.de

FULL PAPER

$$d = \frac{nR}{1-n} \qquad (3)$$

Since the bottom plane is a focal plane, light coming from the same point on this plane will exit the lens in parallel. Moreover, as depicted in Figure 2c, the light rays from a random point in the colored area will be refracted into the left half space, and light from any position within the dark area will go into the right plane. This illustrates the control function of the light propagation with lenticular lenses shown in Figure 2a.

3. Designs and Simulations

As analyzed in Section 2, when colored stripes are correctly placed underneath the lenticular lens array, light rays from different areas are directed into different angular range (Figure 2c). If the black area in Figure 2c is coated with light absorbing materials, while the yellow colored area is coated with any colored reflective materials, the out-coming light from the bottom of a single lens itself is always refracted in the left half plane, which is out of the veiling glare range defined in Figure 1c. This satisfies the antiglare design criteria mentioned in Section 2.

Additional considerations need to be taken into account when using an array of lenses to cover the dashboard. As illustrated in **Figure 3**a, light from the colored stripes can also be refracted into the right half plane by the adjacent lenses. By ray tracing the left- and right-edge positions of the colored stripes, the conditions to avoid veiling glare are $\alpha > \gamma_{max}$ and $\beta < \gamma_{min}$, where α is the minimal refracted angle by the single lens itself for light rays coming from the colored stripe (corresponding to the light coming from the left-edge point of the colored area), β is the maximal angle of refraction by the adjacent lens for colored light rays (corresponding to the light coming from the right-edge position of the colored stripe), and γ_{min}, γ_{max} define the veiling glare range as shown in Figure 1c. By adjusting the position and width of the area of the substrate underneath the lenses, the antiglare condition is

$$\alpha = \arctan\left(\frac{f_2}{a_2 - w/2}\right) \geq \gamma_{max} \qquad (4)$$

$$\beta = \arctan\left(\frac{f_2}{a_1 + w/2}\right) \leq \gamma_{min} \qquad (5)$$

where f_2 is the focal length, w is the period of the lenticular lens array, a_1 and a_2 are the distances from the right and left-edge points of the colored stripe to the right edge of a single lenticular lens, respectively.

An additional consideration is to make the width of the single lens beyond the resolution

capability of human eyes and the lens curves cannot be perceived by our eyes. According to the Rayleigh criterion,[21] the finest feature which naked eyes can resolve at viewing distance of $L = 25$ cm is $L\sin\theta = 1.22L\lambda/D \approx 56$ μm, considering the wavelength of visible light ($\lambda \approx 550$ nm) and the pupil diameter ($D \approx 3$ mm). Assuming $\alpha = \gamma_{max}$ and $\beta = \gamma_{min}$, the largest width of the colored stripe can be obtained from Equations (4) and (5) as

$$a_2 - a_1 = w + \frac{|R|}{n-1}\left(\frac{1}{\tan(\gamma_{max})} - \frac{1}{\tan(\gamma_{min})}\right)$$
$$= 50\,\mu m + \frac{|R|}{0.54}\left(\frac{1}{\tan(\gamma_{min}+30°)} - \frac{1}{\tan(\gamma_{min})}\right) \qquad (6)$$

where $f_2 = |R|/(n-1)$, $w = 50$ μm, refractive index n is set as 1.54 considering that cyclic olefin copolymer (COC) is used for lenticular lens fabrication, and $\gamma_{max} = \gamma_{min} + 30°$ as $\gamma = 2\theta + \varphi$ with φ of ±15°. As depicted in Figure 3b, Equation (6) sets the upper limit of the radius from the condition that $a_2 > a_1$, while the smallest radius is $|R| = w/2$. When the radius is set as the minimal value, i.e., $|R| = w/2$, the colored stripe has the largest width $a_2 - a_1$, which will provide correspondingly highest brightness,
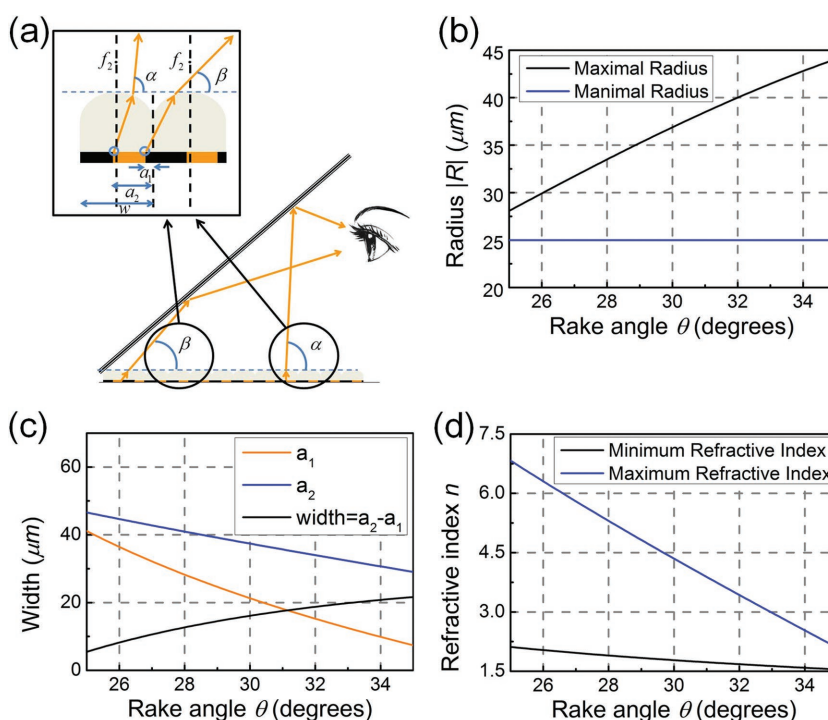
Figure 3. Design criteria for lenticular lens array. a) Analysis of antiglare conditions for lenticular lens array. Two extreme positions on the dashboard are used to analyze the veiling glare range. α is the minimal refracted angle by the single lens itself for light coming from the colored stripe (corresponding to the light coming from the leftmost point of the colored area within one period), β is the maximal angle of refraction by the adjacent lens for colored light rays (corresponding to the light coming from the rightmost position of the colored stripe within one period). b) Maximal and minimal radius $|R|$ of the curved dome dependence on rake angle θ. The minimal value is determined by the lens geometry $|R| \geq w/2$ and the maximal valued of $|R|$ is fixed according to Equation (6) with $a_2 > a_1$. c) Position and width of the colored stripes when $|R| = w/2 = 25$ μm. d) The relation between the refractive index of material n and the rake angle θ. Here the position and width of the colored area is fixed as $a_1 = 7$ μm and $a_2 = 27$ μm.

ADVANCED
MATERIALS
TECHNOLOGIES
www.advmattechnol.de

ADVANCED
SCIENCE NEWS
www.advancedsciencenews.com

FULL PAPER

according to Equation (6). Figure 3c plots the dependence of the largest width of the colored stripe on the rake angle θ varying from 25° to 35° with Equations (4)–(6). It should be noticed that other values within the range calculated in Figure 3b can be selected for $|R|$, and the satisfactory values of a_1 and a_2 can be obtained based on Equations (4) and (5). Finally, the lens material is not restricted to COC but can be other polymeric films. Figure 3d shows the dependence of the refractive index on the rake angle if we assume $a_1 = 7$ μm and $a_2 - a_1 = 20$ μm, which is the calculated result at $\theta = 35°$ in Figure 3c and will also be used for the simulations. All the variations of $|R|$, the colored stripe width $a_2 - a_1$, and n provide more freedom for further designs.

As a specific example, the following parameters are used for detailed discussions: the radius $|R|$ and the period w are set as $|R| = w/2 = 25$ μm so that the curved top surface is exactly a semicylindrical one and the thickness of the lens is determined as $d = 71$ μm with Equation (3). The refractive index of the lens material COC is 1.54. Besides, the position of the colored area is fixed with $a_1 = 7$ μm and $a_2 = 27$ μm, which means the colored area is 20 μm wide and satisfies the conditions of Equations (4)–(6), and the rake angle is assumed as $\theta = 35°$ corresponding to $\gamma_{min} = 55°$ and $\gamma_{max} = 85°$, respectively.
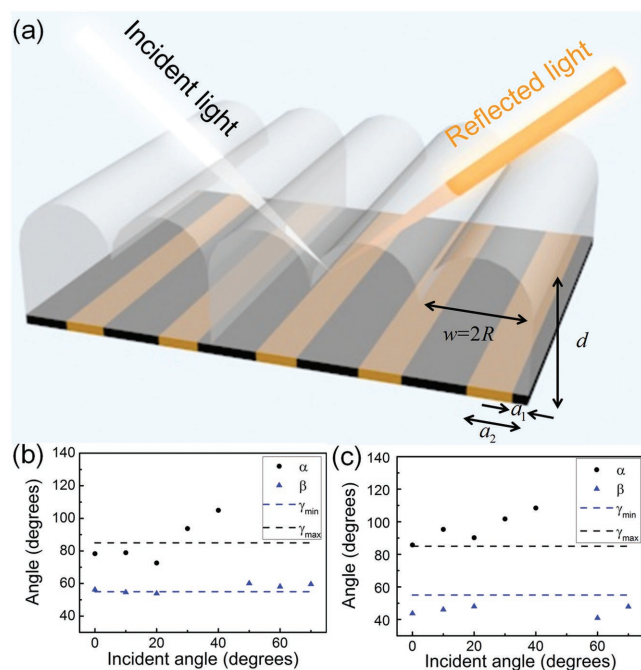
Figure 4. Reflection investigation of the designed lens. a) Designed lenticular lens for the simulation. The reflective area is simulated with the "Mirror" boundary conditions, which will reflect all light rays incident on it. b) Dependence of α (the minimal refraction angle by the single lens itself, black solid circles) and β (the maximal refracted angle by the adjacent lens, blue triangles) on incident angles. Some portion of light will go into the veiling glare range, which is the range between black and blue dashed lines in the plot with $\gamma_{min} = 55°$ and $\gamma_{max} = 85°$, due to the aberration of the lenses. c) Dependence of α (the minimal refraction angle by the single lens itself, black solid circles) and β (the maximal refracted angle by the adjacent lens, blue triangles) on incident angles of the optimized lens. All light rays are controlled out of the veiling glare range and the veiling glare is further reduced.

We use the design summarized above for further simulations using ray tracing software (Zemax, Zemax LLC). All the parameters are shown in **Figure 4**a and the "mirror" boundary condition, which reflects light with ≈95% efficiency, is used to simulate the reflective colored area. Detailed information about the simulation is provided in the Experimental Section. Figure S2 (Supporting Information) shows the light propagation paths after incident on the designed periodic structure from different angles. The minimal refraction angle by the single lens itself α and the maximal refracted angle by the adjacent lens β are highlighted in selected angles, and they are summarized in Figure 4b. Since the simulated structure is based on the theoretical predictions, which assumes the top curvature is very thin, aberrations will occur for light rays incident on the very edge part of the lens. As a result, some light reflected from the reflective area will fall into the veiling glare range ($\gamma_{min} = 55°$ and $\gamma_{max} = 85°$), which can be seen by the dots inside the dashed line range in Figure 4b. At some incident angles, the data for α and β are missed because those light rays get absorbed by the absorber beneath as shown in Figure S2(4)–(8) (Supporting Information).

Practically, the aberrations can be relieved efficiently by slightly reducing the lens thickness. When the lens thickness d is decreased from 71 to 61 μm, all light coming back from the reflective area beneath are well controlled out of the veiling glare range as illustrated in Figure S3 (Supporting Information) and Figure 4c, which efficiently reduces the potential veiling glare after the lens sample being installed in the vehicles. Similarly, those missed data (e.g., from 30° to 70° incident angles) are due to the absorption of the absorber areas. Here, we only consider the case where the drivers are viewing from the middle of vehicles. The definition of veiling glare angular range can also be extended for situations where light rays come from the side with the effective rake angle θ' in the incident plane as shown in Figure S4 (Supporting Information). Then following the design criterion for removing the veiling glare $\alpha > \gamma_{max}$ and $\beta < \gamma_{min}$, satisfactory lens parameters can be obtained with Equations (4)–(6) and veiling glare can be removed by orientating the lens array on the dashboard with the lens length perpendicular to the incident light direction.

4. Lens and Substrate Preparation

Traditionally lenticular lenses can be manufactured via hot melt extrusion using extrusion drums, and such drums are typically made by diamond ruling method.[15,16] However, the typical commercial lenticular lens has period of 250 μm, which cannot satisfy the design criteria described above. We used thermal imprinting method to fabricate the lens array, where the imprinting mold was made by diamond ruling by using an ultraprecision five-axis machining.

A 5 cm × 5 cm size nickel (Ni) hard mold is fabricated for the thermal imprinting of the cylindrical lens array. Two 5 mm wide and 29 μm deep steps are created at both edges of the mold in order to control the final thickness of printed polymer lenses (see the illustration in Figure S5, Supporting Information). Detailed descriptions of the mold preparation are in the Experimental Section.

ADVANCED
SCIENCE NEWS
www.advancedsciencenews.com

ADVANCED
MATERIALS
TECHNOLOGIES
www.advmattechnol.de

FULL PAPER

COC resin is selected as the imprinting material due to its high tensile strength (≈63 MPa) and modulus (≈2.6 GPa), which facilitates handling in the subsequent thin film peeling off and transfer procedures. The COC pellets are spread over a silicon (Si) wafer and pressed into a thin film using another Si wafer as the imprint mold. The Si mold has been coated with self-assembled fluoro-containing monolayers and can be easily separated from the COC film.[22] Subsequently, thermal imprinting with the Ni mold, which is precoated with a silicone releasing layer for surface energy reduction (see the Experimental Section), is operated at 140 °C for 10 min. The microscopic image in **Figure 5**e shows the imprinted lens array has a period of 50 μm. The overall thickness of the lens is well controlled as 61 μm with the 29 μm edge step. Detailed information about the thermal imprinting is provided in the Experimental Section.

For demonstration, a Si substrate is used to make the alternating absorptive/reflective stripe patterns using standard microfabrication facility. A Si wafer is first coated with absorbing materials consisting of multilayer structures with chromium/germanium/silicon/titanium dioxide/magnesium fluoride which provide an averaged absorption >95% across the visible wavelength range.[23,24] Subsequently, the colored stripes are fabricated by photolithography followed by gold (Au) deposition. Other colored materials can also be used. Figure 5f is the microscopic image of the alternating stripe substrate with a pitch of 50 μm and the colored stripe width of 20 μm. Considering the water-repellent property of COC, the peeling-off of the thin lens is done in the water (Figure 5c), which keeps the lens sheet flat and smooth. The alignment of the lens sheet and the absorber/colored stripe substrate is achieved with the help of the morié fringe. The 7 μm offset between the lens and the stripes (i.e., $a_1 = 7$ μm) is aligned under the microscope as shown in Figure S6c (Supporting Information). It is worth noting that even 100 nm pitch mismatch between the lens and absorber/yellow stripe substrate will create the morié fringe which is described in Figure S6d (Supporting Information).

5. Results and Discussion

As can be seen from **Figure 6**a, there is no reflection when the sample is viewed from within the veiling glare range, i.e., the sample renders black, and therefore will not create veiling glare if installed onto the dashboard. A small defected area is circled out in the figure due to the local misalignment which mainly comes from the defects of the lenses during the imprinting/separation process. On the other hand, when the observing angle is out of the veiling glare range, the sample turns bright yellow due to reflection from the Au stripes as shown in Figure 6b. Finally, Figure 6d shows how the sample functions when it is put on a setup that mimics the windshield dashboard in a vehicle (as shown in Figure 6c, the rake angle $\theta = 35°$). Clearly, the area covered by the sample appears bright yellow on the black dashboard, however there is no visible veiling glare from the windshield glass (except the small defected area mentioned in Figure 6a) and we can see through the windshield easily. By comparison, when rotating the sample on the dashboard by 180°, the yellow image from windshield is reflected into our eyes (Figure 6e), which further validates the design of the sample orientation as illustrated in Figure 3a. Due to the small period (≈50 μm) of the lens array, the surface appears very smooth and no lens feature is visible to our eyes (Figure 6a,b). Compared to traditional lenticular lenses, which typically have ≈100 lenses per inch corresponding to ≈250 μm period,[15–17] our fabricated lenses can even be potentially applied for higher resolution displays when integrated with active devices such as light emitting diodes (LEDs).

6. Conclusion

In summary, we demonstrate a lenticular-lens-based design of a colored dashboard which simultaneously offers antiveiling glare applications. The dashboard surface consists of a 50 μm
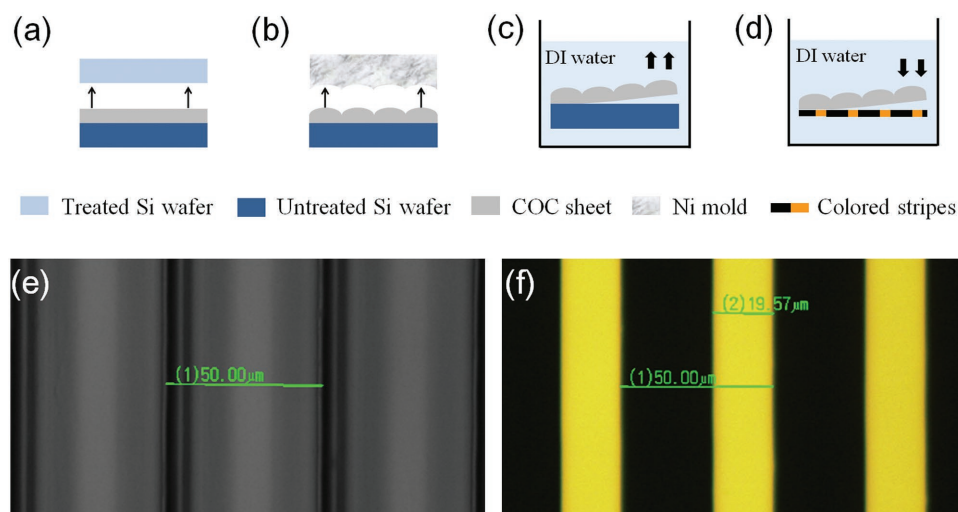
Figure 5. The fabrication process of the lenticular lens array and the alignment with the colored substrate. Due to the hydrophobic property of the COC, the peeling off and the alignment are done in the water, which guarantees lens sheet to be smooth and flat. Panels (e) and (f) are the microscopic images of the imprinted lenses and the colored alternating stripe substrate, respectively.
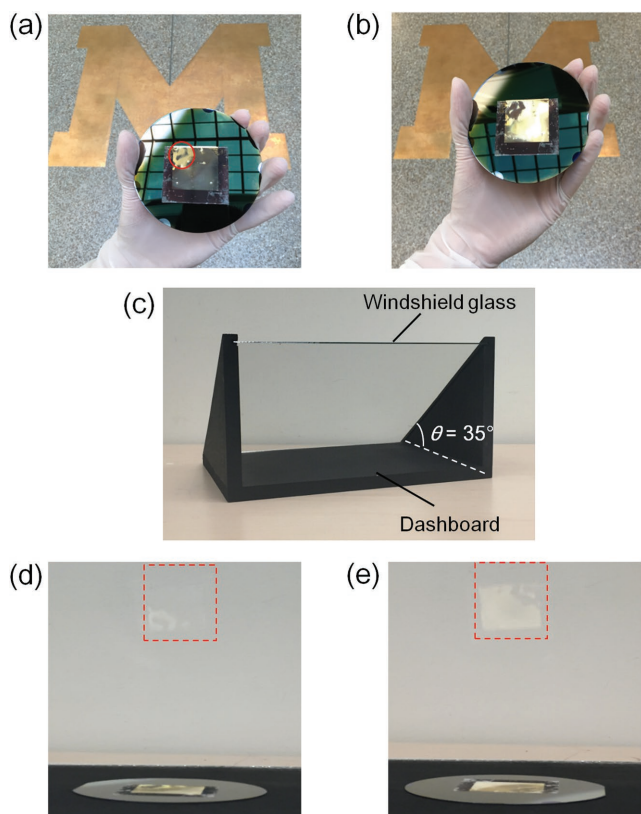
Figure 6. Demonstrations of samples on the windshield-dashboard setup. Panels a) and b) show the final aligned sample when viewed in and out of the veiling glare range, respectively. Panel c) presents the windshield-dashboard setup with the rake angle $\theta = 35°$ for demonstration. The sample renders no reflection into the veiling glare range which is consistent with the prediction by the simulations and does not cause the veiling glare when installed on the dashboard as shown in d). By comparison, projected image of the sample on the windshield is clearly observed if rotating the sample by 180° as presented in e).

period lenticular lens array made of COC material covering a surface of alternating stripes of absorber and reflective colored materials. By accurate design of the lens dimensions, unwanted light reflection from the bottom stripes are well controlled out of the veiling glare range and simultaneously create visual colors to the drivers' eyes. It is worth noting that the mass production can be easily achieved by roll-to-roll imprinting.[25–29] Moreover, the small pitch design can be potentially extended to display systems inside vehicle due to its high resolution in the near future.

7. Experimental Section

Simulations: The lenticular lens arrays are modeled with the Zemax (Zemax LLC) based on ray optics analysis. The unit cell with a 50 µm pitch consists of a semicylinder with the radius of 25 µm atop and a cuboid beneath. The length along the lens lines can be randomly selected as the authors assume it is infinite. The lens is made of COC material with a refractive index around 1.54. Multiple incident light sources are set above the lens array to cover the unit cell for collecting the reflection angle data at different incident angles (from 0° to 70° with an increase step of 10°).

Diamond Machining for Ni Mold: The diamond tool has a arc tip with the arc of 170° and a radius of 25 µm from Contour Fine Tooling Ltd. 200 µm thick Ni is electroplated onto the thick aluminum (Al) plate as the mold material since Ni is much softer when compared to aluminum (Al) and copper (Cu) considering the sharp diamond tip. Using an ultraprecision five-axis machining system (Nanotech 350FG, Moore Nanotechnology Systems LLC), two 29 µm steps are first planed out onto the Ni layer. Then the semicylindrical patterns inversed to the final lenses are created with the semicircle shaped diamond tool.

Thermal Imprinting: Nine cyclic olefin copolymer (COC 8007, TOPAS Advanced Polymers Inc., Florence, Kentucky, USA) pellets are positioned on the untreated Si substrate as a 3×3 array of a 2 cm space and then pressed into a 70 µm thick film at 140 °C for 8 min with 1 ton pressure covered with a Si superstrate. The superstrate is pretreated with fluoro-containing monolayers to facilitate the subsequent demolding process. After separating the substrate and superstrate, the COC film stays on the untreated Si substrate due to its higher surface energy. To further reduce the defects, the film after heat pressing is put into a vacuum chamber at 140 °C for 20 min. After coating a silicone releasing layer (OS-20, Dow Corning Corp.) onto the Ni mold, the thermal imprinting is operated at 140 °C for 10 min with gradually increasing the pressure to 1 ton using the manual hydraulic press (Specac Ltd.), which leaves a residue layer around 7 µm on the very bottom. So the overall thickness is around 61 µm (curved semicircle 25 µm + spacer 29 µm + residue layer 7 µm), which satisfies the simulation design.

Supporting Information

Supporting Information is available from the Wiley Online Library or from the author.

Acknowledgements

[1] H. You, T. Ryu, K. Oh, M.-H. Yun, K.-J. Kim, *Int. J. Ind. Ergon.* **2006**, *36*, 323.

[2] T. Jindo, K. Hirasago, *Int. J. Ind. Ergon.* **1997**, *19*, 105.

[3] E. Bertilsson, E. Svensson, *Master Thesis*, Luleå University of Technology **2009**.

[4] M. L. Mefford, J. F. Michael, A. Go, *Report No. UMTRI-2003-36*, **2003**.

[5] A. Dunsäter, M. Andersson, *Master Thesis*, Linköping University **2008**.

[6] J. Schumann, M. J. Flannagan, M. Sivak, E. C. Traube, *J. Saf. Res.* **1997**, *28*, 133.

[7] J. L. Sauter, N. Bow, M. L. Ladriere, S. C. Parman, *SAE Technical Paper, No. 920105*, **1992**.

[8] C. D. Storms, *SAE Technical Paper No. 940646*, **1994**.

[9] C. H. Munro, *US 8467129*, **2013**.

[10] K. M. Reitz, *US 6299231*, **2001**.

[11] D. Banerjee, L. J. Guo, K.-T. Lee, *US 20160085008*, **2016**.

[12] S. Ahn, J. Cha, H. Myung, S.-M. Kim, S. Kang, *Appl. Phys. Lett.* **2006**, *89*, 213101.

[13] L. J. Guo, *Adv. Mater.* **2007**, *19*, 495.

[14] C. Zhang, H. Subbaraman, Q. Li, Z. Pan, J. G. Ok, T. Ling, C.-J. Chung, X. Zhang, X. Lin, R. T. Chen, L. J. Guo, *J. Mater. Chem. C* **2016**, *4*, 5133.

[15] R. B. Johnson, G. A. Jacobsen, *SPIE Opt. Photonics* **2005**, *5874*, 587406.

[16] R. B. Johnson, *presented at SPIE Int. Opt. Des. Conf. 2006*, Vancouver, BC, Canada, June **2006**.

[17] H. Kim, J. Kim, J. Kim, B. Lee, S.-D. Lee, *Opt. Commun.* **2015**, *357*, 52.

[18] Y. Takaki, N. Nago, *Opt. Express* **2010**, *18*, 8824.

[19] S. Pastoor, M. Wöpking, *Displays* **1997**, *17*, 100.

[20] C. Van Berkel, D. W. Parker, A. R. Franklin, *presented at SPIE*, San Jose, CA, USA, April **1996**.

[21] M. Born, E. Wolf, *Principles of Optics*, 7th ed., Cambridge University Press, New York, NY **1999**.

[22] M. Beck, M. Graczyk, I. Maximov, E.-L. Sarwe, T. Ling, M. Keil, L. Montelius, *Microelectron. Eng.* **2002**, *61*, 441.

[23] K.-T. Lee, C. Ji, L. J. Guo, *Appl. Phys. Lett.* **2016**, *108*, 031107.

[24] C. Yang, C. Ji, W. Shen, K.-T. Lee, Y. Zhang, X. Liu, L. J. Guo, *ACS Photonics* **2016**, *3*, 590.

[25] S. H. Ahn, L. J. Guo, *Adv. Mater.* **2008**, *20*, 2044.

[26] S. H. Ahn, L. J. Guo, *ACS Nano* **2009**, *3*, 2304.

[27] C. Stuart, Y. Chen, *ACS Nano* **2009**, *3*, 2062.

[28] M. K. Kwak, J. G. Ok, J. Y. Lee, L. J. Guo, *Nanotechnology* **2012**, *23*, 344008.

[29] J. G. Ok, M. K. Kwak, C. M. Huard, H. S. Youn, L. J. Guo, *Adv. Mater.* **2013**, *25*, 6554.